Racetrack Computing with a Topological Boundary Ratchet

Parisa Omidvar,[1] Markus Bestler,[2] Sima Zahedi Fard,[1] Oded Zilberberg,[2,*] and Marc Serra-Garcia[1,†]
[1]AMOLF, Science Park 104, 1098 XG Amsterdam, The Netherlands
[2]Department of Physics, University of Konstanz, D-78457 Konstanz, Germany

(Received 30 September 2025; revised 10 February 2026; accepted 9 March 2026; published 21 April 2026)

Multistable order parameters provide a natural means of encoding nonvolatile information in spatial domains, a concept that forms the foundation of magnetic memory devices. However, this stability inherently conflicts with the need to move information around the device for processing and readout. While in magnetic systems, domains can be transported using currents or external fields, mechanisms to robustly shuttle information-bearing domains across neutral systems are scarce. Here, we experimentally realize a topological boundary ratchet in an elastic metamaterial, where digital information is encoded in buckling domains and transported in a quantized manner via cyclic loading. The transport is topological in origin: neighboring domains act as different topological pumps for their Bogoliubov excitations, so their interface hosts topological boundary modes. Cyclic loading renders these modes unstable through interdomain pressure, which in turn drives the motion of the domain wall. We demonstrate that the direction of information propagation can be controlled through adjustable mechanical constraints on the buckling beams, and numerically investigate buckling-based domain-wall logic circuits in an elastic metamaterial network. The underlying tight-binding structure with low-order nonlinearities makes this approach a general pathway toward racetrack memories in neutral systems.

DOI: 10.1103/jw9p-s3kk

The separation of memory and computation, known as the von Neumann bottleneck [1], represents a major inefficiency in modern computer architectures and has been estimated to account for up to 90% of the energy cost of contemporary AI training [2]. Efforts to overcome this bottleneck by integrating memory and computation have motivated the development of racetrack memories [3–8]. In these devices, information is stored in magnetic domains or skyrmions and can be transported and manipulated using injected currents or external fields. Moving to neutral, nonmagnetic systems, such coupling to external fields is missing, and topological pumping [9–13] arose as a mechanism for controllable information transport. However, such pumps adiabatically move linear excitations, which are short-lived [14–16]. Hence, mechanisms to transport persistently stored information in a controllable way are still missing.

Our experiment involves a nonlinear elastic metamaterial [17–22] that persistently stores information, and robustly transports it under an external cyclic load. This process is driven by sequential instabilities occurring in localized modes at the boundaries between spatial domains. Our racetrack memory is a chain of interconnected beams [Figs. 1(a) and 1(b)], which were cut from a thin polymer sheet. We create a sublattice potential on the chain by applying a strong compressive displacement β_1 at one end of every alternate beam. These beams exhibit two stable buckling states, labeled as 0 and 1, which can store information. Beams experiencing lower compression β_2 do not store information, and serve instead as variable couplings. We refer to the beams under high compression as main beams and those under low compression as coupling beams. The racetrack can support different spatial domains, where a domain corresponds to a region in the chain with all the main beams uniformly assuming the values of 0 or 1. Between these regions, domain walls appear. By soliton, we dub a domain of 1 surrounded by two domains of 0.

To introduce directed soliton motion, we apply an additional compressive displacement in the beams, of the form $\pm\alpha \sin[\theta(t)]$ [Fig. 1(a)]. This force alternates sign every two sites, being positive in one pair of coupling-main beams, and negative in the next. This time-dependent compression spatially repeats every four sites, defining a four-site unit cell. When the lattice is modulated, by increasing θ over time, domain walls and therefore solitons are transported through the system [Fig. 1(c) and Supplemental Material [23], movies 1 and 2], demonstrating the elastic racetrack memory functionality. If the static compressive displacements β_1 and β_2 are exchanged, the direction of propagation reverses [Fig. 1(d)], providing a

*Contact author: oded.zilberberg@uni-konstanz.de
†Contact author: m.serragarcia@amolf.nl

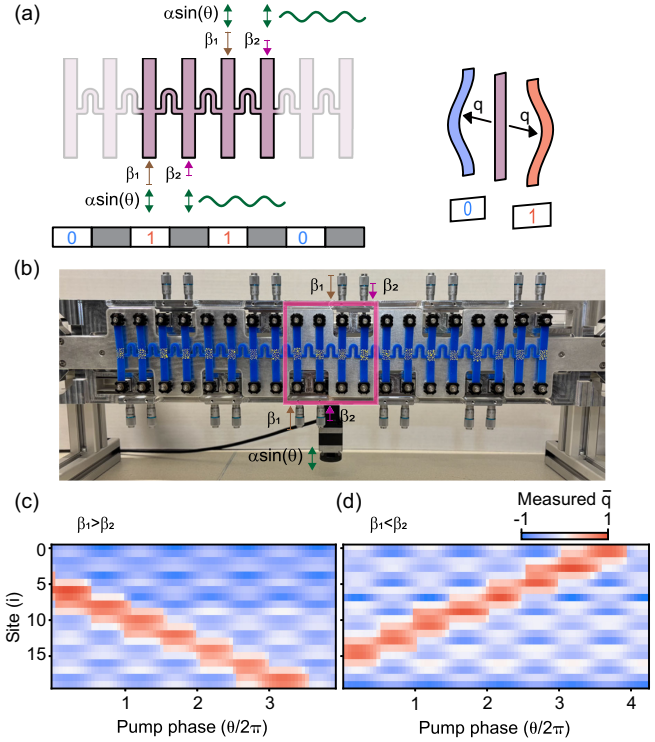

FIG. 1. Observation of quantized information transport in an elastic racetrack memory. (a) Sketch of the metamaterial consisting of beams coupled with arced connections. The beams are subject to a constant (dc) and a time-varying (ac) compression (pink and green arrows, respectively). Every four sites, the compression pattern repeats, forming a unit cell. The beams under higher compression are bistable most of the time and have two stable buckling shapes (red and blue). These two configurations can represent binary digits 0 and 1, allowing the beams to store information like bits in a memory array. (b) Polymer sheet assembled on the setup, the pink rectangle marks the unit cell of the structure. (c),(d) Measured normalized displacements at the centers of the beams ($\bar{q}$) as the ac compression is varied, for two different dc compression β_j. The pumping starts from a configuration containing one soliton. After a full cycle of the external compression pattern, the soliton is shifted by one unit cell.

mechanism to read out the information by changing the boundary conditions. In our experiment, the time-dependent compression is applied by clamping the alternating ends of the beams to a moving plate, that is driven by a single motor [Fig. 1(b)].

Our soliton displacement stems from the motion of the two domain walls defining it. Hence, we turn to investigate the mechanism driving the domain wall motion. Our elastic racetrack memory [Fig. 1(a)] is a nonlinear perturbative metamaterial [34,35] governed by the tight-binding potential [Fig. 2(a)]

$$V = \sum_{n,j}\left[\frac{\lambda}{4}q_{n,j}^4 + \frac{1}{2}(\omega_0^2 + a_{0,j} + a_{1,j}(\theta))q_{n,j}^2\right] + \sum_l \frac{c}{2}(q_l - q_{l+1})^2, \quad (1)$$

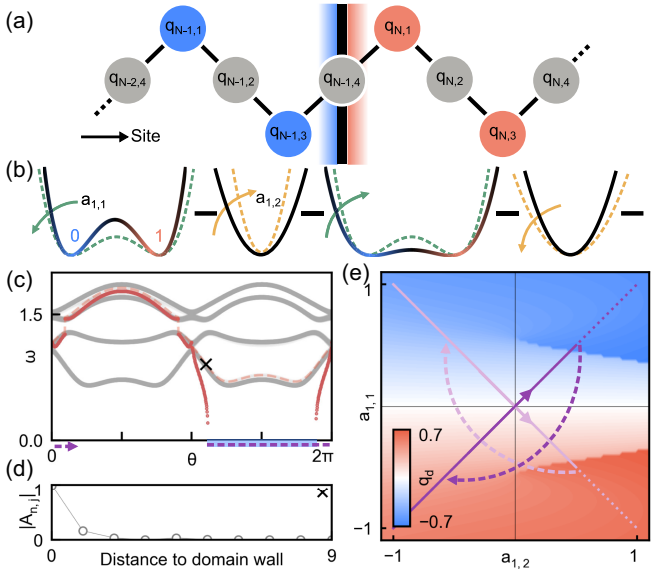

FIG. 2. Theory of soliton movement. (a) Sketch of the tight-binding model corresponding to the experiment in Figs. 1(a)–1(c), described by Eq. (1), including a domain wall (black vertical line in the middle). Gray circles stand for monostable sites while red (blue) circles depict bistable sites initialized in the 1 (0) state. (b) Onsite potentials (black lines) of the 4 sites of the unit cell as θ is varied. The effect of larger $a_{1,1}$ ($a_{1,2}$) on the main (coupling) beams is marked as green (yellow) dashed lines. Horizontal black lines display coupling between the potentials. (c) Band structure (gray) of Bogoliubov excitations on top of the red domain from (a) during one pump cycle of θ, with $a_{1,1} = a_{1,2} = -\sin(\theta)$ for a racetrack of 80 sites with $\lambda = 1$, $c = 0.25$, $\omega_0^2 = 2$, $a_{0,1} = -3$, and $a_{0,2} = -0.5$. Boundary mode frequencies when coupled to vacuum (dashed red) and to the second domain (red dots). Regions where the frequencies coupled to the second domain turn imaginary (unstable) are marked in blue. Encountering instabilities shifts θ by π (purple dashed arrow). (d) Mode shape $|A_{n,j}|$ (see Supplemental Material [23]) for a localized fluctuation mode of the unperturbed red domain from (a) for 10 sites and $\theta \approx 1.1\pi$ marked with a black cross in (c). Site 0 corresponds to site $q_{N,1}$. (e) Instability phase diagram for same parameters as in (c) for a racetrack of 16 sites. Red (blue) regions indicate where the blue (red) domain becomes unstable. The dark purple line shows the pump trajectory in our system, where θ advances by π when reaching an instability due to modified boundary conditions (dashed arrow). Hence, the pump cycle never reaches a part of the pump cycle (dotted line). Exchanging β_1 and β_2 effectively leads to a new pump cycle on top of the instability diagram (light purple).

with center displacement $q_{n,j}$ of the j th beam ($j \in \{1,2,3,4\}$) in the n th unit cell, quartic nonlinearity λ, and harmonic potential with natural frequency ω_0. The system is spatially modulated by the constant compressive displacements β, which introduce tight-binding potential terms $a_{0,j} = \pm\gamma\beta$ due to geometric nonlinearity, quantified by γ [36]. Similarly, the pumping phase (θ)-dependent compressive displacements introduce tight-binding potential terms of the form $a_{1,j}(\theta) = \pm\gamma\alpha\sin(\theta)$. Figure 2(b) shows the resulting

modulation of the local potential as θ is varied. Nearest neighbors are attractively coupled with constant $c > 0$. For compact notation, we let l index all pairs of i and j, with $l + 1$ corresponding to the next site in the racetrack. The static compressive displacements are chosen such that $a_{0,1} = a_{0,3}$ and $a_{0,2} = a_{0,4}$. The quadratic term of each site, $\frac{1}{2}(a_0 + a_1(\theta) + \omega_0^2 + 2c)q_i^2$, is negative (positive) for the first and third (second and fourth) site of the unit cell. As a result, main (bistable) and coupling (monostable) sites alternate along the racetrack. In the experiment, we vary the compressive displacements with the pumping phase such that $a_{1,1} = -a_{1,3}$ and $a_{1,2} = -a_{1,4}$ [cf. Figs. 1(a) and 1(b) with Fig. 2(b)]. In the following theory analysis, we first assume that $a_{1,1}$ and $a_{1,2}$ can be independently tuned.

The metamaterial model (1) can be viewed as a nonlinear extension of a topological pump, owing to the four-site periodic modulation of the local harmonic potential [10–16,37]. We investigate the domain wall motion mechanism by calculating the Bogoliubov modes of the system, the spectrum of linearized fluctuations around a many-body equilibrium configuration. On a single domain, the linearized Bogoliubov excitation modes can acquire a nontrivial Chern number when $a_{1,1}(\theta)$ and $a_{1,2}(\theta)$ are varied independently (see Supplemental Material [23]). One might therefore expect the quantized soliton motion to originate from the topology of the Bogoliubov modes, cf. Refs. [38,39]. However, when $a_{1,1}(\theta)$ and $a_{1,2}(\theta)$ are tuned simultaneously as in the experiment, the Bogoliubov bulk bands close during the pump cycle and the Chern number becomes ill-defined, see Fig. 2(c). Nonetheless, at points along the pump cycle, where the excitation gaps remain open, boundary modes still manifest in the gaps [Fig. 2(d)] due to nonvanishing bulk polarization that develops as θ is varied [40].

To trace the origin of soliton motion, we numerically simulate a system with a single domain wall [Fig. 2(a)]. For each point in the $a_{1,1}$–$a_{1,2}$ plane, the system is initialized in a single-domain-wall state and allowed to relax to equilibrium. The wall displacement is quantified by $q_d = (q_{N-1,3} + q_{N,1})/2$ [Fig. 2(e)]. Values near zero indicate stability, while values approaching ± 0.7 mark domain wall motion: the wall relaxes to a shifted single-wall state, with the sign of q_d determining the direction. This identifies a so-called *topological ratchet* mechanism [41]. In this mechanism, instabilities in the Bogoliubov spectrum result in growing localized fluctuations that trigger domain wall motion. This mechanism stands in contrast with the adiabatic spectral flow, governed by the Chern number transport, that characterizes traditional topological pumps. Consequently, although the experimental scan of θ traces a straight line in the $a_{1,1}$–$a_{1,2}$ plane (with bulk-band closings at the origin), it encounters only a single instability, enforcing unidirectional wall motion. This yields quantized transport controlled by a single parameter. Furthermore, reversing the boundary conditions (β_1 and β_2) as in

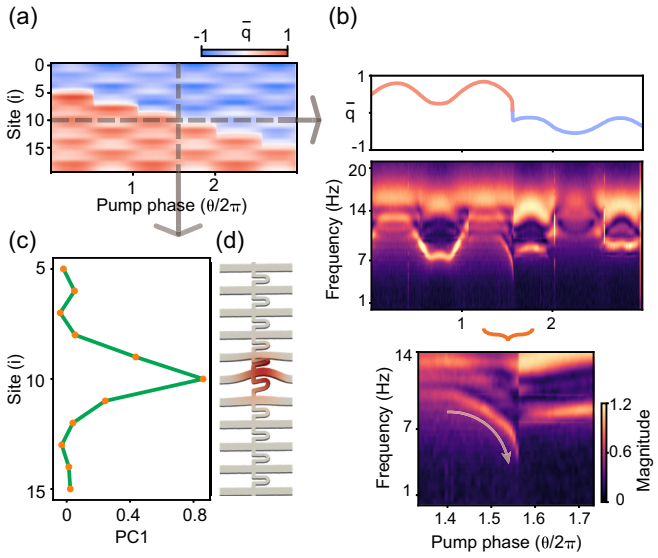

FIG. 3. Experimental imaging of the Bogoliubov spectrum during domain wall propagation. (a) Measured normalized displacements of the beams with a varying compression displacement. The initial configuration of the sample consists of a single domain wall that propagates throughout the experiment. (b) Buckling displacement (top) and the frequency response (bottom) of the 10th beam in different stages of the experiment. The inset zooms in on the region when the beam transitions (or "hops") between its two stable states. At this moment, the frequency of the mode drops close to zero. (c) Mode shape imaging of the structure at the moment of the 10th beam's transition, obtained using principal component analysis (PCA). The mode is strongly localized at the transitioning beam, confirming that the destabilization corresponds to a localized mode, which allows the domain wall to move forward. (d) First mode shape of the system, simulated using the finite element method (FEM) at a selected moment corresponding to the 10th beam's transition. The simulation shows the same localization as observed in (c).

Figs. 1(c) and 1(d) interchanges main and coupling sites. In tight-binding language, this maps $a_{0,1} \to a_{0,2}$ and $a_{0,2} \to a_{0,1}$ and mirrors the unit cell. We therefore reverse the propagation direction of the domain wall.

Although distinct from a conventional topological pump, the ratchet mechanism remains topologically rooted. Analyzing excitations on a racetrack with a domain wall reveals boundary modes localized at the interdomain boundary as θ varies. Unlike a vacuum boundary, the opposing domain exerts an additional "pressure" [42], which can destabilize the boundary mode (see Supplemental Material [23] and Ref. [41]). As shown in Fig. 2(c), this pressure softens the boundary-mode frequency. If this softening is strong enough to induce an instability on the boundary mode, the resulting unstable dynamics cause the wall to shift by two sites (one main beam, one coupling beam). Each displacement of the domain wall modifies its boundary condition, equivalent to advancing the pumping phase θ by π [Figs. 2(c) and 2(e)]

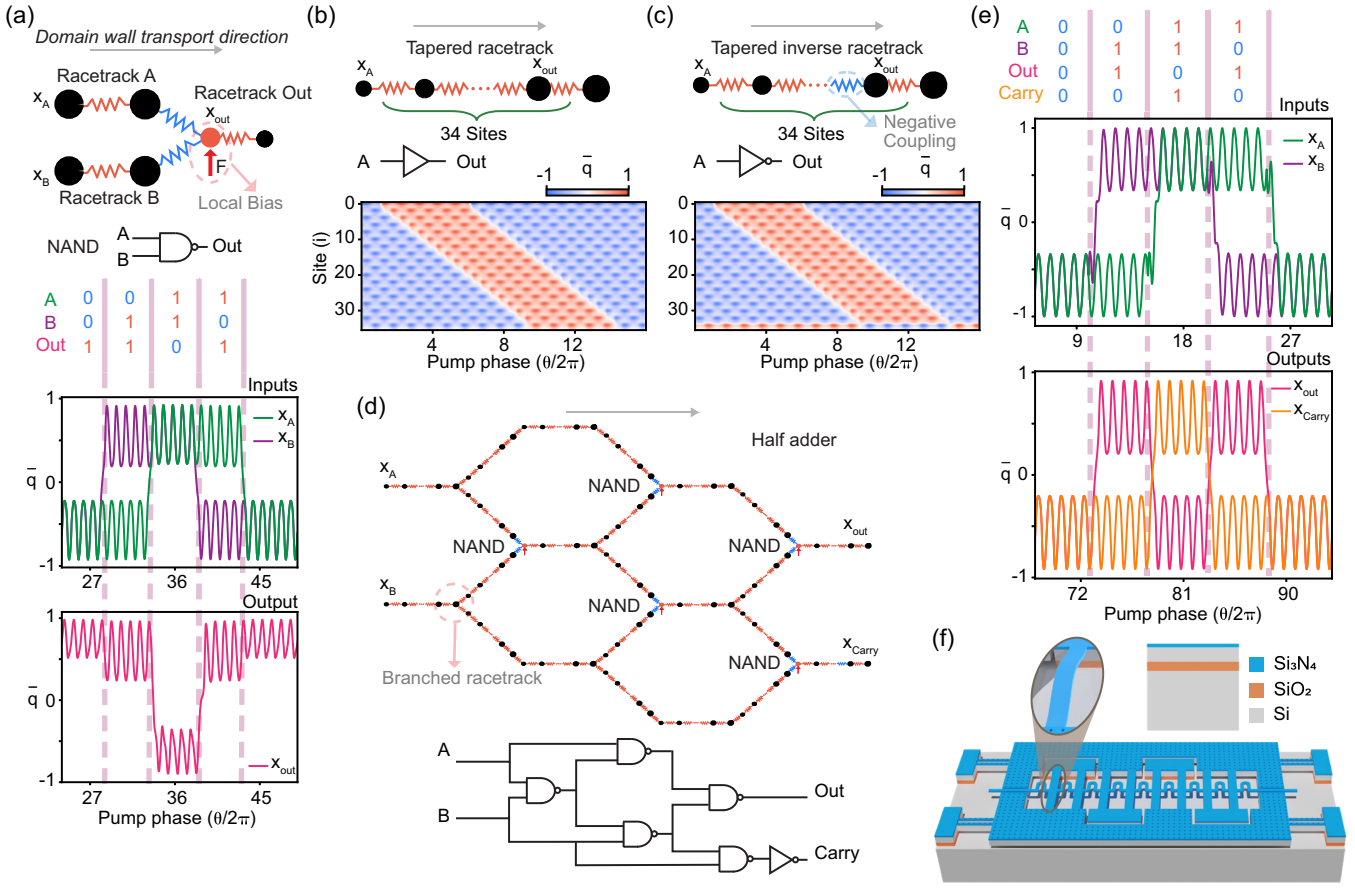

FIG. 4. Numerical investigation of domain wall logic. (a) Simulation of a NAND logic gate using the unit cell in Fig. 2(b). The gate has two input racetrack (A), (B) with a softer output racetrack. The local positive force breaks the symmetry of output's potential (the red arrow), biasing it toward state 1. The blue springs represent effective negative coupling. The two graphs show the computed normalized displacement of output and inputs, accurately reflecting NAND logic. The positive displacement values correspond to logical 1, and the negative values correspond to logical 0. (b) Top: Tapered racetrack design enabling signal transfer from a softer input site to a stiffer output site, which functions as buffer and amplifier. Bottom: Signal propagation through the racetrack. (c) Top: Tapered inverse racetrack that inverts the transmitted signal from the input to the output. This is achieved by using an effective negative coupling between the input and output sites, functioning as logical NOT gate. Bottom: Inverted signal propagation in the racetrack. (d) Top: Honeycomb-shaped design of a half adder constructed from cascading the elastic logic elements, including buffer, NOT, and NAND gates. To form the honeycomb layout, branching is introduced at selected points along the racetracks. Bottom: The corresponding symbolic logic diagram. (e) Truth table of a half adder accompanied by the graphs illustrating computed normalized displacements of the input and the output sites in the honeycomb-shaped design. The half adder takes two one-digit binary inputs [(A) and (B)] and adds them into a two-digit binary output representing the sum (out) and carry. (f) 3D sketch of the device layout on a silicon wafer. This conceptual sketch highlights that if the device is miniaturized at microscale, the layout remains planar and fabrication friendly.

[11,41]. There are thus two essential ingredients for topologically directed domain wall motion: First, the presence of localized boundary modes of topological nature at the domain walls, and, second, the existence of interactions between domains that soften these boundary modes causing instabilities for specific values of the pump angle θ. The location of the boundary modes and when they can be destabilized via pressure determine the direction of domain wall and soliton motion (see Supplemental Material [23]).

To test this hypothesis, we designed a new experiment to probe and observe the destabilization of the localized boundary mode. We initialize the metamaterial in a configuration containing two domains separated by a domain wall [Fig. 3(a)]. Then, we measure the fluctuation spectrum at the central beam ($i = 10$), by introducing small broadband excitations into the system and Fourier transforming the resulting beam vibration (see Supplemental Material [23] for experimental details). During the measurement, we continuously increase θ, causing the domain wall to propagate. The results are shown in Fig. 3(b). When the domain wall is far away from the central beam, the spectrum displays the Bogoliubov bulk bands on top of the domain where the central beam resides; their frequencies are modulated by the variable compression of the beam. However, when the domain wall approaches the central beam, we observe an additional peak in the spectrum,

whose frequency goes to zero right before the domain wall advances. A modal frequency going to zero is indicative of the stiffness becoming negative, and provides an experimental signature of the instability that drives domain wall motion. To confirm that this additional peak corresponds to a localized boundary mode, we perform a complementary experiment, where the domain wall remains fixed at the center site, and we measure the fluctuation response of each individual beam. From this scanning measurement, we reconstruct the mode profile using principal component analysis [43,44]. The results reveal that the observed additional peak is indeed localized at the domain wall [Fig. 3(c)], and its existence can also be corroborated via the finite element method simulations [Fig. 3(d)].

The racetrack memory introduced here enables the construction of logic gates and circuits by forming branched networks. Here, we will explore this possibility via numerical simulations. Although there is no fundamental limitation to experimentally realizing racetrack logic circuits, our tabletop demonstrator platform is too large to realize a full circuit within our experimental capabilities. Figure 4(a) illustrates the operation of a universal NAND gate. The gate connects the last sites of two "input" racetracks to the first site of an "output" racetrack via an effective negative coupling in the tight-binding description. Such negative couplings represent an inversion of the motion direction, and do not imply the existence of negative energy or thermodynamic instabilities. They have been realized, for example, using appropriately placed levers [45] or via magnetic elements [46]. These terms are essential for the realization of universal logic: The output of certain gates, such as NOT, NAND, or NOR moves in the opposite direction than the input, requiring the presence of a displacement-inverting coupling. To realize NAND behavior, the output site is biased toward positive buckling, ensuring a logical 1 whenever the two inputs oppose and cancel each other. Reliable operation requires the output racetrack to be softer than the inputs; otherwise, it would perturb their dynamics. We achieve this by scaling its tight-binding parameters by 0.125. For scalability, we implement a tapered transition between input and output stiffnesses over 36 sites [Figs. 4(b) and 4(c)]. This design allows arbitrary logic circuits, as any digital circuit can be planarized using crossover gadgets [47]. We demonstrate this by constructing a two-bit adder [Figs. 4(d) and 4(e)]. Although these simulations are based on a tight-binding model, negative couplings and branching geometries can be physically implemented (see Ref. [35]), and the required biases are experimentally accessible (see Supplemental Material [23]).

Our results illustrate how a robust information transfer mechanism, based on nonlinear topological ratchets, can act as an enabler for novel forms of physical information processing [48,49]. For example, in mechanical computers [50,51], prior realizations of digital computations with buckling elements required resetting the device after every iteration [17,52,53] or, due to beam asymmetries, only enabled the transmission of specific buckling states [17]. In contrast, our metamaterial can operate on a continuous input stream of information. Although our tabletop demonstrator operates on timescales of seconds, its unique ability to combine information storage and computing in a single elastic structure can find applications in devices such as zero-power event-counting sensors. Moreover, the design introduced here is planar, and thus compatible with conventional microfabrication processes [Fig. 4(f)], where frequencies can be much higher [54], and the operation energy is extremely low [55]; in fact, at small scales, energies associated to buckling can approach the thermal scale limit k_BT [55]—providing a novel platform to study the thermodynamics of computation. Since the physics of our device is captured by a generic tight-binding model, we anticipate that these capabilities can be extended to other deformation modes, such as flexural and torsional deformations [56,57]. In fact, it may even be possible to observe similar information propagation mechanisms in photonic systems, for example, by leveraging parametric bistabilities [58] or multiple colocated degrees of freedom [59] as binary variables.

Acknowledgments—The authors are grateful to Martin van Hecke, Ewold Verhagen, Bernat Dura Faulí, Saeed Zohoori, Finn Bohte and Théophile Louvet for valuable inputs and discussions. The authors thank AMOLF's support department: Henk-Jan Bolujit for the design and preparation of the experimental setup; Precision Manufacturing group, particularly Olaf Janssen and Mark Willemse, for fabrication of the setup and assistance with sample preparation; and Peter van Eijden for his technical assistance with the experiment. This work was supported by the ERC under Grant No. 101040117 (INFOPASS). Additional funding was provided by the Deutsche Forschungsgemeinschaft (DFG) through Projects No. 449653034, No. 521530974, and No. 545605411, as well as via SFB 1432 (Project No. 425217212). We also acknowledge support from the Swiss National Science Foundation (SNSF) through the Sinergia Grant No. CRSII5_206008/1 and the NCCR SPIN. Funded by the European Union.

Views and opinions expressed are, however, those of the author(s) only and do not necessarily reflect those of the European Union or the European Research Council Executive Agency. Neither the European Union nor the granting authority can be held responsible for them.

Data availability—The data that support the findings of this article are openly available [60].

[1] J. Backus, Commun. ACM **21**, 613 (1978).

[2] K. Bourzac, Nature (London), 10.1038/d41586-024-03408-z (2024).
[3] M. Hayashi, L. Thomas, R. Moriya, C. Rettner, and S. S. Parkin, Science **320**, 209 (2008).
[4] S. S. Parkin, M. Hayashi, and L. Thomas, Science **320**, 190 (2008).
[5] Z. Luo, A. Hrabec, T. P. Dao, G. Sala, S. Finizio, J. Feng, S. Mayr, J. Raabe, P. Gambardella, and L. J. Heyderman, Nature (London) **579**, 214 (2020).
[6] V. T. Pham, N. Sisodia, I. Di Manici, J. Urrestarazu-Larrañaga, K. Bairagi, J. Pelloux-Prayer, R. Guedas, L. D. Buda-Prejbeanu, S. Auffret, A. Locatelli *et al.*, Science **384**, 307 (2024).
[7] K. Gu, Y. Guan, B. K. Hazra, H. Deniz, A. Migliorini, W. Zhang, and S. S. Parkin, Nat. Nanotechnol. **17**, 1065 (2022).
[8] A. Szameit and M. C. Rechtsman, Nat. Phys. **20**, 905 (2024).
[9] M. J. Rice and E. J. Mele, Phys. Rev. Lett. **49**, 1455 (1982).
[10] D. J. Thouless, Phys. Rev. B **27**, 6083 (1983).
[11] Y. E. Kraus, Y. Lahini, Z. Ringel, M. Verbin, and O. Zilberberg, Phys. Rev. Lett. **109**, 106402 (2012).
[12] M. Lohse, C. Schweizer, O. Zilberberg, M. Aidelsburger, and I. Bloch, Nat. Phys. **12**, 350 (2016).
[13] R. Citro and M. Aidelsburger, Nat. Rev. Phys. **5**, 87 (2023).
[14] Y. Xia, E. Riva, M. I. Rosa, G. Cazzulani, A. Erturk, F. Braghin, and M. Ruzzene, Phys. Rev. Lett. **126**, 095501 (2021).
[15] M. Jürgensen, S. Mukherjee, and M. C. Rechtsman, Nature (London) **596**, 63 (2021).
[16] M. Jürgensen, S. Mukherjee, C. Jörg, and M. C. Rechtsman, Nat. Phys. **19**, 420 (2023).
[17] L. J. Kwakernaak and M. van Hecke, Phys. Rev. Lett. **130**, 268204 (2023).
[18] X. Fang, D. Yu, J. Wen, Y. Dai, M. R. Begley, H. Gao, and P. Gumbsch, Nature (London) **639**, 639 (2025).
[19] G. Bordiga, E. Medina, S. Jafarzadeh, C. Bösch, R. P. Adams, V. Tournat, and K. Bertoldi, Nat. Mater. **23**, 1486 (2024).
[20] P. Ducarme, B. Weber, M. van Hecke, and J. T. Overvelde, Proc. Natl. Acad. Sci. U.S.A. **122**, e2423301122 (2025).
[21] B. Florijn, C. Coulais, and M. van Hecke, Phys. Rev. Lett. **113**, 175503 (2014).
[22] K. Huang, Y. Lin, Y. Lai, and X. Liu, Chin. Phys. B **33**, 104301 (2024).
[23] See Supplemental Material at http://link.aps.org/supplemental/10.1103/jw9p-s3kk for numerical and experimental methods and additional derivations, which includes Refs. [24–33].
[24] G. E. Uhlenbeck and L. S. Ornstein, Phys. Rev. **36**, 823 (1930).
[25] A. Rößler, SIAM J. Numer. Anal. **48**, 922 (2010).
[26] M. W. Scroggs, I. A. Baratta, C. N. Richardson, and G. N. Wells, J. Open Source Software **7**, 3982 (2022).
[27] M. S. Alnæs, A. Logg, K. B. Ølgaard, M. E. Rognes, and G. N. Wells, ACM Trans. Math. Softw. **40**, 1 (2014).
[28] I. A. Baratta, J. P. Dean, J. S. Dokken, M. Habera, J. HALE, C. N. Richardson, M. E. Rognes, M. W. Scroggs, N. Sime, and G. N. Wells, DOLFINx: The next generation FEniCS problem solving environment (2023), https://zenodo.org/records/18101307.
[29] M. W. Scroggs, J. S. Dokken, C. N. Richardson, and G. N. Wells, ACM Trans. Math. Softw. **48**, 1 (2022).
[30] A. N. Gent, Rubber Chem. Technol. **31**, 896 (1958).
[31] G. Chen, Y. Long, S. Yao, S. Tang, J. Luo, H. Wang, Z. Zhang, and H. Jiang, Nat. Commun. **16**, 1449 (2025).
[32] D. H. Alsem, R. Timmerman, B. L. Boyce, E. A. Stach, J. T. M. De Hosson, and R. O. Ritchie, J. Appl. Phys. **101**, 013515 (2007).
[33] Y. Hatsugai and T. Fukui, Phys. Rev. B **94**, 041102(R) (2016).
[34] K. H. Matlack, M. Serra-Garcia, A. Palermo, S. D. Huber, and C. Daraio, Nat. Mater. **17**, 323 (2018).
[35] S. Z. Fard, P. Tiso, P. Omidvar, and M. Serra-Garcia, arXiv:2509.01625.
[36] M. Serra-Garcia, A. Foehr, M. Molerón, J. Lydon, C. Chong, and C. Daraio, Phys. Rev. Lett. **117**, 010602 (2016).
[37] M. Jürgensen and M. C. Rechtsman, arXiv:2502.14046.
[38] M. Jürgensen and M. C. Rechtsman, Phys. Rev. Lett. **128**, 113901 (2022).
[39] N. Mostaan, F. Grusdt, and N. Goldman, Nat. Commun. **13**, 5997 (2022).
[40] R. Resta and D. Vanderbilt, Theory of polarization: A modern approach, in *Physics of Ferroelectrics: A Modern Perspective* (Springer, Berlin, Heidelberg, 2007), pp. 31–68.
[41] M. Bestler and O. Zilberberg, arXiv:2508.12101.
[42] J. Kellendonk, J. Phys. A **37**, L161 (2004).
[43] S. Han and B. Feeny, Mech. Syst. Signal Process. **17**, 989 (2003).
[44] G. Kerschen, J.-c. Golinval, A. F. Vakakis, and L. A. Bergman, Nonlinear Dyn. **41**, 147 (2005).
[45] R. Süsstrunk and S. D. Huber, Science **349**, 47 (2015).
[46] A. O. Oyelade, Z. Wang, and G. Hu, Theor. Appl. Mech. Lett. **7**, 17 (2017).
[47] A. A. Cantu, A. Luchsinger, R. Schweller, and T. Wylie, Algorithmica **83**, 531 (2021).
[48] H. Jaeger, B. Noheda, and W. G. Van Der Wiel, Nat. Commun. **14**, 4911 (2023).
[49] M. Aifer, Z. Belateche, S. Bramhavar, K. Y. Camsari, P. J. Coles, G. Crooks, D. J. Durian, A. J. Liu, A. Marchenkova, A. J. Martinez *et al.*, arXiv:2507.10463.
[50] H. Yasuda, P. R. Buskohl, A. Gillman, T. D. Murphey, S. Stepney, R. A. Vaia, and J. R. Raney, Nature (London) **598**, 39 (2021).
[51] A. Alù, A. F. Arrieta, E. Del Dottore, M. Dickey, S. Ferracin, R. Harne, H. Hauser, Q. He, J. B. Hopkins, L. P. Hyatt *et al.*, Smart Mater. Struct. **34**, 063501 (2025).
[52] T. Mei and C. Q. Chen, Nat. Commun. **14**, 5204 (2023).
[53] T. Mei, Z. Meng, K. Zhao, and C. Q. Chen, Nat. Commun. **12**, 7234 (2021).
[54] D. Garcia-Sanchez, A. San Paulo, M. J. Esplandiu, F. Perez-Murano, L. Forró, A. Aguasca, and A. Bachtold, Phys. Rev. Lett. **99**, 085501 (2007).
[55] S. Stuij, J. M. van Doorn, T. Kodger, J. Sprakel, C. Coulais, and P. Schall, Phys. Rev. Res. **1**, 023033 (2019).
[56] Y. Lai, Y. Wu, P. Sheng, and Z.-Q. Zhang, Nat. Mater. **10**, 620 (2011).
[57] G. Ma, C. Fu, G. Wang, P. Del Hougne, J. Christensen, Y. Lai, and P. Sheng, Nat. Commun. **7**, 13536 (2016).
[58] J. Kellner, A. Sabatti, A. Maeder, and R. Grange, Optica **12**, 702 (2025).
[59] T. Song, Y. Jing, C. Shen, H. Chu, J. Luo, R. Jia, C. Wang, M. Xiao, Z.-Q. Zhang, R. Peng *et al.*, Nat. Commun. **16**, 8915 (2025).
[60] P. Omidvar, M. Bestler, S. Zahedi Fard, O. Zilberberg, and M. Serra-Garcia, "Replication package for Racetrack computing with a topological boundary ratchet," 10.5281/zenodo.19268308 (2026).